

Tri-timescale Beamforming Design for Tri-hybrid Architectures with Reconfigurable Antennas

Mengzhen Liu, *Graduate Student Member, IEEE*, Ming Li, *Senior Member, IEEE*, Rang Liu, *Member, IEEE*, and Qian Liu, *Member, IEEE*

Abstract—Reconfigurable antennas possess the capability to dynamically adjust their fundamental operating characteristics, thereby enhancing system adaptability and performance. To fully exploit this flexibility in modern wireless communication systems, this paper considers a novel tri-hybrid beamforming architecture, which seamlessly integrates pattern-reconfigurable antennas with both analog and digital beamforming. The proposed tri-hybrid architecture operates across three layers: (i) a radiation beamformer in the electromagnetic (EM) domain for dynamic pattern alignment, (ii) an analog beamformer in the radio-frequency (RF) domain for array gain enhancement, and (iii) a digital beamformer in the baseband (BB) domain for multi-user interference mitigation. To establish a solid theoretical foundation, we first develop a comprehensive mathematical model for the tri-hybrid beamforming system and formulate the signal model for a multi-user multi-input single-output (MU-MISO) scenario. The optimization objective is to maximize the sum-rate while satisfying practical constraints. Given the challenges posed by high pilot overhead and computational complexity, we introduce an innovative tri-timescale beamforming framework, wherein the radiation beamformer is optimized over a long-timescale, the analog beamformer over a medium-timescale, and the digital beamformer over a short-timescale. This hierarchical strategy effectively balances performance and implementation feasibility. Simulation results validate the performance gains of the proposed tri-hybrid architecture and demonstrate that the tri-timescale design significantly reduces pilot overhead and computational complexity, highlighting its potential for future wireless communication systems.

Index Terms—Reconfigurable antennas, tri-hybrid beamforming, tri-timescale, hybrid beamforming.

I. INTRODUCTION

Future wireless communication systems are expected to leverage ultra-wide spectrum resources in high-frequency bands, such as millimeter wave (mmWave), to accommodate the growing demand for ultra-high data rates [1]. To mitigate the severe propagation loss in these frequency bands, massive multiple-input multiple-output (mMIMO) systems or extremely large antenna arrays (ELAA) are typically employed to ensure reliable signal transmission [2]. In conventional antenna arrays, each antenna element typically exhibits a fixed and identical radiation patterns that concentrate energy towards predetermined directions, often perpendicular to the array. Within this framework, most existing studies focus on signal

processing-based beamforming techniques, which adjust the phase and amplitude of signals across antenna elements to direct beam towards specific directions.

However, the limitations of conventional pattern-fixed antennas are becoming increasingly apparent in emerging applications, such as ELAA and near-field communications [3]. Specifically, system performance is significantly influenced not only by array beamforming but also by the radiation gain of each individual antenna element. While antennas with narrow, highly energy-concentrated radiation patterns provide high gain within specific angular ranges, they suffer substantial performance degradation in the endfire direction due to a sharp decrease in signal strength. Conversely, antennas with broader radiation patterns provide wider coverage at the cost of reduced gain, ultimately compromising the quality of service.

Reconfigurable antenna technology offers a promising solution to the challenges faced by conventional pattern-fixed antennas by enhancing adaptability [4]-[7]. Reconfigurable antennas can adapt their internal parameters to modify key operating characteristics such as radiation patterns [8]-[10], frequency responses [11], and polarizations [12], [13]. Among these, radiation pattern reconfiguration is particularly crucial for wireless communication systems, as it directly impacts both the transmitted and received signal strength. To enable flexible control over these characteristics, several hardware implementations have been developed, such as electronically steerable parasitic array radiator (ESPAR) antennas [14], frequency selective surfaces (FSS) [15], and pixel antennas [16], all of which share similar underlying principles and architectures. Typically, a reconfigurable antenna consists of an active element and multiple parasitic elements, where the connection states of parasitic elements are dynamically controlled to alter the current distribution within the antenna, thereby modifying its electromagnetic (EM) properties. This capability introduces new degrees of freedom (DoF) in the EM domain, offering the potential to overcome existing performance limitations and enable more efficient wireless communication systems.

With significant advancements in reconfigurable antenna technology, integrating pattern-reconfigurable antennas into antenna arrays has gained considerable attention in recent years. For instance, the authors in [17] employ multi-port network theory and beamspace channel representation to develop an EM-based communication model for pixel antennas, which is then used to optimize antenna coding for maximizing channel gain. A similar approach is applied in [14] to construct an ESPAR antenna model, enabling analysis and optimization of ESPAR beamforming. Additionally, the authors in [18]

M. Liu and M. Li are with the School of Information and Communication Engineering, Dalian University of Technology, Dalian 116024, China (e-mail: liumengzhen@mail.dlut.edu.cn, mli@dlut.edu.cn).

R. Liu is with the Center for Pervasive Communications and Computing, University of California, Irvine, CA 92697, USA (e-mail: rangl2@uci.edu).

Q. Liu is with the School of Computer Science and Technology, Dalian University of Technology, Dalian 116024, China (e-mail: qianliu@dlut.edu.cn).

introduce a decomposition method based on spherical harmonic functions to model radiation patterns in the EM domain. This approach decomposes the radiation pattern into a linear combination of orthogonal bases, facilitating the iterative design of radiation patterns and digital precoders. While these studies highlight the advantages of replacing conventional pattern-fixed antennas with innovative pattern-reconfigurable ones, they overlook the significant hardware costs and power consumption incurred by the increasing number of antennas and operating frequencies. To tackle these issues, existing literature commonly suggests hybrid beamforming architectures for mMIMO systems, as a power-efficient alternative to conventional fully-digital beamforming [19].

In hybrid beamforming, analog beamforming controls the beam direction in the radio frequency (RF) domain, while digital beamforming performs spatial signal processing in the baseband (BB) domain, leveraging a reduced number of RF chains and hardware-efficient phase shifters (PSs). Common hybrid beamforming architectures, including fully-connected [20], partially-connected [21], and dynamic architectures [22], strike a balance between performance and implementation cost. While recent advances in hardware and power-efficient hybrid architectures have enabled large-scale MIMO deployments for 6G and beyond, the limitations of conventional pattern-fixed antennas remain a significant challenge. To address this issue, we propose leveraging the flexibility of pattern-reconfigurable antenna technology to address the performance degradation caused by fixed radiation patterns, while utilizing hybrid beamforming to reduce power consumption without sacrificing performance.

In this paper, we consider a novel tri-hybrid beamforming architecture that integrates pattern-reconfigurable antennas with both analog and digital beamforming. Specifically, this tri-hybrid architecture consists of three layers: A radiation beamformer in the EM domain to align radiation patterns with desired direction, an analog beamformer in the RF domain to enhance array gain, and a digital beamformer in the BB domain to mitigate multi-user interference. The concept of tri-hybrid architecture was first introduced in [23], [24]. While prior analyses and simulations have demonstrated the advantages of tri-hybrid beamforming in terms of spectral efficiency and energy consumption, several critical issues must be addressed before its practical implementation in future wireless systems. First, accurate acquisition of instantaneous channel state information (CSI) becomes more challenging due to the higher dimensionality of CSI and the limited number of RF chains, leading to increased pilot overhead and requiring advanced estimation algorithms. Second, optimizing the beamformers across all three domains is more complicated due to parameter coupling, discrete phase-shift constraints, and the nonlinear characteristics of reconfigurable antennas, etc.

Recently, a two-timescale framework has been proposed to address system overhead and design complexity in conventional hybrid beamforming. In this framework, the analog beamformer is optimized based on channel statistics over a long-timescale, while the digital beamformer is designed using low-dimensional instantaneous effective CSI over a short-timescale [25]-[27]. Building on this concept and leverag-

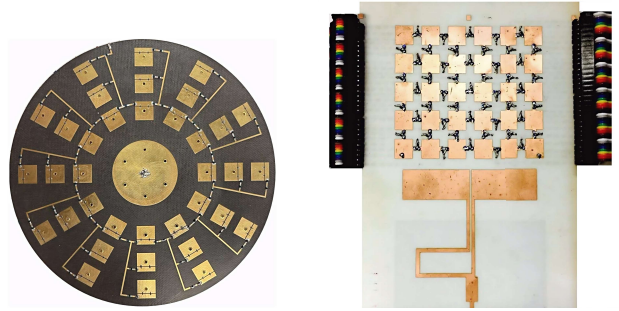


Fig. 1. The hardware prototypes of pattern-reconfigurable antenna (left [8], right [9]).

ing the unique characteristics of the tri-hybrid architecture, we propose a novel tri-timescale framework for tri-hybrid beamforming design, effectively managing practical overhead and complexity. The main contributions of this paper are summarized as follows:

- We first develop a comprehensive mathematical model for the radiation beamformer based on multiple pattern-reconfigurable antennas, along with the corresponding virtual angular index channel in the EM domain. Building upon this model, we derive the formulation of the tri-hybrid beamforming architecture, establish the signal model for a multi-user multiple-input single-output (MUMISO) system employing this architecture, and present the associated optimization problem.
- For the tri-hybrid beamforming design, our objective is to maximize the sum-rate while satisfying constraints on radiation pattern energy, constant modulus and discrete phase shifts of PSs, a non-overlapping dynamic connection network, and the total transmit power budget. To effectively address the challenges of high pilot overhead and substantial computational complexity, we propose a novel tri-timescale beamforming framework, where the radiation beamformer is optimized over a long-timescale, the analog beamformer over a medium-timescale, and the digital beamformer over a short-timescale.
- Extensive simulations are conducted to validate the capability of the tri-hybrid beamforming architecture in enhancing system performance, as well as the effectiveness of the proposed tri-timescale beamforming design algorithm in reducing pilot overhead and computational complexity.

Notations: Boldface lower-case and upper-case letters indicate column vectors and matrices, respectively. $(\cdot)^*$, $(\cdot)^T$, and $(\cdot)^H$ denote the conjugate, transpose, and transpose-conjugate. $|a|$, $\|\mathbf{a}\|$, and $\|\mathbf{A}\|_F$ are the magnitude of scalar a , the norm of vector \mathbf{a} , and the Frobenius norm of matrix \mathbf{A} . $\text{vec}(\mathbf{A})$ stacks \mathbf{A} 's columns into a long column vector. Notation \otimes is the Kronecker product of matrices. $\text{blkdiag}\{\mathbf{A}_1, \mathbf{A}_2, \dots, \mathbf{A}_M\}$ denotes a block diagonal matrix. $\mathbf{1}_M$ and \mathbf{I}_M represent an $M \times 1$ vector of ones and an $M \times M$ identity matrix, respectively. $\Re\{\cdot\}$ denotes the real part of a complex number. The statistical expectation is given by $\mathbb{E}\{\cdot\}$. $\mathbf{a}(i)$ denotes the i -th entry of the vector \mathbf{a} . $\mathbf{A}(i, \cdot)$ and $\mathbf{A}(i, j)$ denote the i -th row and (i, j) -th element of matrix \mathbf{A} , respectively.

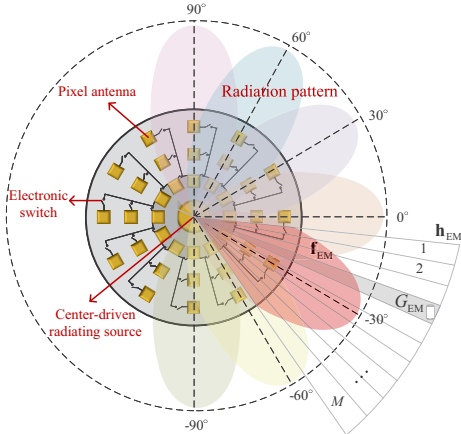


Fig. 2. The illustration of a pattern-reconfigurable antenna.

II. SYSTEM MODEL AND PROBLEM FORMULATION

A. Pattern-reconfigurable Antenna

Pattern-reconfigurable antenna is an advanced technology that enables dynamic adaptation of radiation patterns to enhance signal quality, mitigate interference, and improve coverage in wireless communication systems. Various hardware implementations have been explored to achieve flexible radiation pattern control, including ESPAR antennas [14], FSS [15], and pixel antennas [16]. Among these, pixel antenna technology has emerged as the most practical and versatile solution for integration into compact antenna arrays. The hardware prototypes of pixel-based reconfigurable antennas are illustrated in Fig. 1.

Having demonstrated their feasibility in real-world applications, we now describe the hardware configuration and operational principle of the pixel-based pattern-reconfigurable antennas. As illustrated in Fig. 2, pixel antenna technology discretizes a continuous antenna surface into electrically small parasitic elements, called pixels, with a central radiating source driving the entire antenna. These pixels serving as fundamental building blocks, utilize low-voltage, binary-controlled pin diodes to connect or disconnect adjacent pixels. By adjusting the states of these switches, different pixel topologies are formed, which modify the current distribution across the antenna surface. This reconfiguration alters the electric and magnetic field components radiated by the antenna, enabling the generation of a diverse set of radiation patterns.

To evaluate the performance improvements brought by pattern-reconfigurable antennas, it is crucial to establish a mathematical model for both the radiation pattern and the corresponding channel characteristics. As aforementioned, pattern-reconfigurable antennas introduce an additional DoF in the EM domain, effectively expanding the information coverage dimension of conventional antennas, from a one-dimensional spatial representation to an M -dimensional angular information, where M represents the number of uniform sampling points in the angular domain. Specifically, a single reconfigurable radiation pattern (exemplified by the red pattern in Fig. 2) is characterized over M discrete directions in the EM

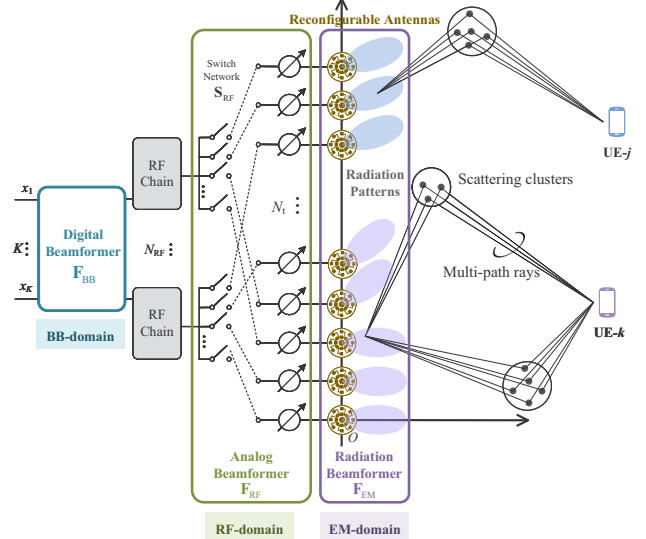


Fig. 3. Tri-hybrid beamforming architecture.

domain and is represented by $\mathbf{f}_{EM} \in \mathbb{R}^M$, with each element corresponding to the radiation gain in a specific direction. To model reception characteristics, we introduce the virtual angular index channel for the pattern-reconfigurable antenna, denoted as $\mathbf{h}_{EM} \in \{0, 1\}^M$, which serves as an index matrix indicating the spatial angles at which the user is located. Consequently, the effective gain in the EM domain can be expressed as $G_{EM} = \mathbf{h}_{EM}^H \mathbf{f}_{EM}$, which quantifies the radiation intensity directed toward the user's actual spatial angle. By optimizing the radiation pattern \mathbf{f}_{EM} to align with the angular domain channel characteristics, the correlation between them can be maximized, leading to enhanced radiation efficiency. This formulation serves as the foundation for the following theoretical analysis and optimization.

Inspired by the increased design DoF introduced by pattern-reconfigurable antennas, we integrate this advanced hardware component into the conventional hybrid beamforming architecture and propose a tri-hybrid beamforming framework that incorporates beamforming across three domains. Specifically, radiation beamforming in the EM domain is employed to dynamically shape the radiation pattern, analog beamforming in the RF domain is utilized to enhance array gain, and digital beamforming in the BB domain is implemented to mitigate multi-user interference.

B. Tri-hybrid Beamforming Architecture

To provide a clear illustration of the proposed tri-hybrid beamforming architecture, we consider a mmWave MU-MISO downlink communication system, as shown in Fig. 3. Specifically, a base station (BS) equipped with a uniform linear array (ULA) serves multiple single-antenna user equipments (UEs). The BS employs reconfigurable antennas that dynamically adjust their radiation patterns, while each UE is equipped with a conventional omnidirectional antenna. The antenna spacing at the BS is set to $d = \lambda/2$, where λ is the center carrier

wavelength. Let $\mathcal{N}_t \triangleq \{1, 2, \dots, N_t\}$ denote the set of BS antennas, $\mathcal{K} \triangleq \{1, 2, \dots, K\}$ denote the set of UEs, and $\mathcal{L} \triangleq \{1, 2, \dots, L\}$ denote the set of propagation paths between the BS and each UE. In the following, we mathematically formulate the radiation beamformer \mathbf{F}_{EM} in the EM domain, the analog beamformer \mathbf{F}_{RF} in the RF domain and the digital beamformer \mathbf{F}_{BB} in the BB domain, establishing the foundation for the tri-hybrid beamforming architecture.

EM domain: Building upon the radiation pattern model of a single pattern-reconfigurable antenna \mathbf{f}_{EM} presented in Section II-A, we extend this model to characterize the programmable radiation pattern of the entire antenna array at the BS, which consists of N_t reconfigurable antennas. The resulting radiation beamformer in the EM domain is expressed in the following matrix form

$$\mathbf{F}_{\text{EM}} \triangleq \text{blkdiag}\{\mathbf{f}_{\text{EM},1}, \mathbf{f}_{\text{EM},2}, \dots, \mathbf{f}_{\text{EM},N_t}\} \in \mathbb{R}^{MN_t \times N_t}, \quad (1)$$

where the m -th element of $\mathbf{f}_{\text{EM},n}$ represents the radiation gain of the n -th antenna in the m -th angular direction. To ensure fairness in pattern design, the total energy of each antenna's radiation pattern is restricted and normalized as $\|\mathbf{f}_{\text{EM},n}\|^2 = 1, \forall n$. To further characterize the spatial mapping of the reconfigurable antennas, we introduce the virtual angular index channel matrix

$$\overline{\mathbf{H}}_{\text{EM},k} \triangleq \mathbf{I}_{N_t} \otimes \mathbf{H}_{\text{EM},k} \in \{0, 1\}^{MN_t \times LN_t}, \quad \forall k, \quad (2)$$

where $\mathbf{H}_{\text{EM},k} \triangleq [\mathbf{h}_{\text{EM},k,1}, \mathbf{h}_{\text{EM},k,2}, \dots, \mathbf{h}_{\text{EM},k,L}] \in \{0, 1\}^{M \times L}$ that specifies the spatial angles associated with the k -th UE. Each column $\mathbf{h}_{\text{EM},k,l}$ contains exactly one non-zero element, indicating the angular direction of the l -th propagation path for the k -th UE. Consequently, the radiation gain $\mathbf{G}_{\text{EM},k} \in \mathbb{R}^{LN_t \times N_t}$ of all antennas towards the k -th UE can be formulated as

$$\begin{aligned} \mathbf{G}_{\text{EM},k} &= \overline{\mathbf{H}}_{\text{EM},k}^H \mathbf{F}_{\text{EM}} \\ &= \text{blkdiag}\{\mathbf{H}_{\text{EM},k}^H \mathbf{f}_{\text{EM},1}, \dots, \mathbf{H}_{\text{EM},k}^H \mathbf{f}_{\text{EM},N_t}\}, \end{aligned} \quad (3)$$

where the l -th entry of $\mathbf{H}_{\text{EM},k}^H \mathbf{f}_{\text{EM},n}$ represents the actual radiation gain of the n -th antenna towards the l -th direction for the k -th UE. In summary, the matrices \mathbf{F}_{EM} and $\overline{\mathbf{H}}_{\text{EM},k}$ mathematically capture the additional degrees of freedom introduced by reconfigurable antennas, enabling a more flexible and adaptive radiation beamforming strategy in the EM domain.

RF domain: We adopt a dynamic-subarray analog beamforming architecture, where each RF chain is adaptively connected to a disjoint subset of the total transmit antennas via a switch network. By fully exploiting the design flexibility of dynamic antenna selection, this architecture achieves an optimal balance between system efficiency and communication performance. Without loss of generality, we assume that the number of RF chains N_{RF} is not less than the number of UEs K , i.e., $N_{\text{RF}} \geq K$, and the set of RF chains is denoted as $\mathcal{N}_{\text{RF}} \triangleq \{1, 2, \dots, N_{\text{RF}}\}$. The analog beamformer employs a set of low-resolution PSs, each following a constant modulus constraint with quantized phase control of B bits. The discrete phase set of PSs is given by $\mathcal{F} \triangleq \{\frac{1}{\sqrt{N_t}} e^{j\frac{2\pi b}{2^B}} | b =$

$0, 1, \dots, 2^B - 1\}$. To facilitate dynamic-subarray beamforming, we define the analog beamformer matrix as $\mathbf{F}_{\text{RF}} \in \{\mathcal{F}, 0\}^{N_t \times N_{\text{RF}}}$, which implies that if the l_{RF} -th RF chain is connected to the n -th antenna, the corresponding phase-shift takes a non-zero value, i.e., $\mathbf{F}_{\text{RF}}(n, l_{\text{RF}}) \in \mathcal{F}$; if not, it is set as zero, i.e., $\mathbf{F}_{\text{RF}}(n, l_{\text{RF}}) = 0$. Moreover, to ensure non-overlapping subarrays, each antenna is dynamically assigned to only one RF chain, meaning that the analog beamformer matrix is restricted to have only one non-zero element per row, i.e., $\|\mathbf{F}_{\text{RF}}(n, :)\|_0 = 1$.

BB domain: We exploit the digital beamformer $\mathbf{F}_{\text{BB}} \triangleq [\mathbf{f}_{\text{BB},1}, \mathbf{f}_{\text{BB},2}, \dots, \mathbf{f}_{\text{BB},K}] \in \mathbb{C}^{N_{\text{RF}} \times K}$ to pre-process transmitted signals in the BB domain, addressing the limitation of having fewer RF chains, which restricts direct control over each antenna's signal. This procedure effectively mitigates multi-user interference and enhances overall system performance.

C. Channel Model

After establishing the mathematical formulation of the tri-hybrid beamforming architecture, our focus now shifts to developing a comprehensive channel model that accommodates the expanded dimensionality introduced by the pattern-reconfigurable antenna array. Specifically, unlike conventional channel models that primarily account for path loss and spatial phase gradients, the proposed model incorporates the virtual angular index channel matrix $\overline{\mathbf{H}}_{\text{EM},k}, \forall k$ in (2). This integration enables an explicit representation of the angular characteristics of each propagation path. Furthermore, when combined with the radiation beamformer \mathbf{F}_{EM} in (1), it enables the determination of the radiation intensity $\mathbf{G}_{\text{EM},k}, \forall k$ in (3), facilitating a more precise characterization of the system's electromagnetic behavior.

To establish a foundation for the innovative channel model of the pattern-reconfigurable antenna array, we first present the traditional mmWave channel model. Due to the sparse scattering characteristics of the mmWave band, the channel typically consists of a few dominant clusters, each containing multiple propagation paths [28]. Let $\mathcal{C} \triangleq \{1, 2, \dots, C\}$ denote the set of scattering clusters, and $\mathcal{L}_c \triangleq \{1, 2, \dots, L_c\}$ denote the set of multi-path rays within the c -th scattering cluster. The channel between the n -th antenna and the k -th UE can be expressed as

$$h_{k,n} = \sum_{c=1}^C \sum_{l_c=1}^{L_c} \alpha_{k,c,l_c} e^{-j\frac{2\pi}{\lambda}(n-1)d \sin \theta_{k,c,l_c}}, \quad \forall k, n, \quad (4)$$

where θ_{k,c,l_c} and α_{k,c,l_c} denote the angle of departure (AoD) and channel gain corresponding to the l_c -th ray in the c -th scattering cluster, respectively. The AoD θ_{k,c,l_c} can be described as

$$\theta_{k,c,l_c} = \bar{\theta}_{k,c} + \Delta\theta_{k,l_c}, \quad \forall k, c, l_c, \quad (5)$$

where $\bar{\theta}_{k,c}$ denotes the nominal AoD of the c -th scattering cluster for the k -th UE, and $\Delta\theta_{k,l_c}$ denotes the angular deviation of the l_c -th ray from the nominal direction, following Gaussian distribution $\Delta\theta_{k,l_c} \sim \mathcal{N}(0, \varsigma_{k,c}^2)$, with $\varsigma_{k,c}$ indicating the angle spread. The channel gain involves the typically distance-dependent path loss with r_{k,c,l_c} representing

the propagation distance. It follows the same modeling as in (5), i.e., $r_{k,c,l_c} = \bar{r}_{k,c} + \Delta r_{k,l_c}$, where $\Delta r_{k,l_c} \sim \mathcal{N}(0, l_{k,c}^2)$. For better clarity in the subsequent channel model formulation, we define $L \triangleq \sum_{c=1}^C L_c$ as the total number of paths. With this notation, the channel model in (4) can be reformulated in a more compact form as follows

$$h_{k,n} = \sum_{l=1}^L \alpha_{k,l} e^{-j\frac{2\pi}{\lambda}(n-1)d \sin \theta_{k,l}}, \quad \forall k, n. \quad (6)$$

Furthermore, the integration of pattern-reconfigurable antennas extends the channel representation from a one-dimensional to an M -dimensional formulation by incorporating additional EM domain channel information, i.e., $\bar{\mathbf{H}}_{\text{EM},k}, \forall k$ in (2). Specifically, the dimension-extended channel for the n -th pattern-reconfigurable antenna, denoted as $\mathbf{h}_{k,n} \in \mathbb{C}^M$, is expressed as follows

$$\mathbf{h}_{k,n} = \sum_{l=1}^L (\alpha_{k,l} e^{-j\frac{2\pi}{\lambda}(n-1)d \sin \theta_{k,l}}) \otimes \mathbf{h}_{\text{EM},k,l}, \quad \forall k, n. \quad (7)$$

Following this formulation, by stacking the channel vectors $\mathbf{h}_{k,n}, \forall n$ of all N_t antennas, we obtain the complete channel vector for the k -th UE, given by $\mathbf{h}_k \triangleq [\mathbf{h}_{k,1}^T, \mathbf{h}_{k,2}^T, \dots, \mathbf{h}_{k,N_t}^T]^T \in \mathbb{C}^{MN_t}$. The corresponding expression can be explicitly formulated as

$$\mathbf{h}_k = \sum_{l=1}^L (\alpha_{k,l} \mathbf{a}_{k,l}) \otimes \mathbf{h}_{\text{EM},k,l}, \quad \forall k, \quad (8)$$

where

$$\mathbf{a}_{k,l} \triangleq [1, e^{-j\frac{2\pi}{\lambda}d \sin \theta_{k,l}}, \dots, e^{-j\frac{2\pi}{\lambda}(N_t-1)d \sin \theta_{k,l}}]^T, \quad \forall k, l, \quad (9)$$

denotes the steering vector. By applying the Kronecker product formula and rearranging the order of summation, (8) can be equivalently expressed as

$$\mathbf{h}_k = \text{vec}(\mathbf{H}_{\text{EM},k} \mathbf{H}_{\text{S},k}^T), \quad \forall k, \quad (10)$$

with

$$\mathbf{H}_{\text{S},k} = [\alpha_{k,1} \mathbf{a}_{k,1}, \alpha_{k,2} \mathbf{a}_{k,2}, \dots, \alpha_{k,L} \mathbf{a}_{k,L}] \in \mathbb{C}^{N_t \times L}, \quad \forall k, \quad (11)$$

representing the spatial domain channel. Additionally, to enhance clarity and brevity, the EM domain channel and spatial domain channel can be separated into two independent multiplicative expressions, which yields

$$\mathbf{h}_k = \bar{\mathbf{H}}_{\text{EM},k} \bar{\mathbf{h}}_{\text{S},k}, \quad \forall k, \quad (12)$$

where $\bar{\mathbf{H}}_{\text{EM},k} \in \{0, 1\}^{MN_t \times LN_t}$ is defined in (2) containing the EM domain channel information, and $\bar{\mathbf{h}}_{\text{S},k} \triangleq \text{vec}(\mathbf{H}_{\text{S},k}^T) \in \mathbb{C}^{LN_t}$ includes the spatial domain channel information.

D. System Model

In the MU-MISO downlink system shown in Fig. 3, the transmitted signal is first processed by the digital beamformer \mathbf{F}_{BB} in the BB domain, followed by the analog beamformer \mathbf{F}_{RF} in the RF domain and subsequently shaped by the radiation beamformer \mathbf{F}_{EM} in the EM domain, before being

radiated by the pattern-reconfigurable antennas. After propagating through the spatial channel, it is finally received by the UE. Based on the above mathematical definition, the signal received by the k -th UE is given by

$$y_k = \bar{\mathbf{h}}_{\text{S},k}^H \bar{\mathbf{H}}_{\text{EM},k}^H \mathbf{F}_{\text{EM}} \mathbf{F}_{\text{RF}} \mathbf{F}_{\text{BB}} \mathbf{x} + n_k, \quad \forall k, \quad (13)$$

where $\mathbf{x} \triangleq [x_1, x_2, \dots, x_K]^T \in \mathbb{C}^K$ denotes the transmitted symbols of K UEs that satisfies $\mathbb{E}\{\mathbf{x}\mathbf{x}^H\} = \mathbf{I}_K$, and $n_k \sim \mathcal{CN}(0, \sigma_k^2)$ denotes the additive white Gaussian noise (AWGN) at the k -th UE. The signal-to-interference-plus-noise ratio (SINR) of the k -th UE can be calculated as

$$\text{SINR}_k = \frac{|\bar{\mathbf{h}}_{\text{S},k}^H \bar{\mathbf{H}}_{\text{EM},k}^H \mathbf{F}_{\text{EM}} \mathbf{F}_{\text{RF}} \mathbf{f}_{\text{BB},k}|^2}{\sum_{j=1, j \neq k}^K |\bar{\mathbf{h}}_{\text{S},k}^H \bar{\mathbf{H}}_{\text{EM},k}^H \mathbf{F}_{\text{EM}} \mathbf{F}_{\text{RF}} \mathbf{f}_{\text{BB},j}|^2 + \sigma_k^2}, \quad \forall k, \quad (14)$$

and the corresponding achievable rate can be calculated as

$$R_k = \log_2(1 + \text{SINR}_k). \quad (15)$$

E. Problem Formulation

In this paper, based on the tri-hybrid beamforming architecture, we propose to jointly design the radiation beamformer \mathbf{F}_{EM} in the EM domain, the analog beamformer \mathbf{F}_{RF} in the RF domain, and the digital beamformer \mathbf{F}_{BB} in the BB domain to maximize the sum-rate, while satisfying the constraints of radiation pattern energy, constant modulus and discrete phases of PSs, non-overlapping dynamic connection network, and total transmit power budget. Thus, the joint three domain beamformer optimization problem with full instantaneous CSI is formulated as

$$\max_{\mathbf{F}_{\text{EM}}, \mathbf{F}_{\text{RF}}, \mathbf{F}_{\text{BB}}} \sum_{k=1}^K R_k \quad (16a)$$

$$\text{s.t.} \quad \|\mathbf{f}_{\text{EM},n}\|^2 = 1, \quad \forall n, \quad (16b)$$

$$\mathbf{F}_{\text{RF}}(n, l_{\text{RF}}) \in \{\mathcal{F}, 0\}, \quad \forall n, l_{\text{RF}}, \quad (16c)$$

$$\|\mathbf{F}_{\text{RF}}(n, :)\|_0 = 1, \quad \forall n, \quad (16d)$$

$$\|\mathbf{F}_{\text{RF}} \mathbf{F}_{\text{BB}}\|_F^2 \leq P_t, \quad (16e)$$

where P_t is the transmit power budget.

Within this tri-hybrid beamforming architecture, accurately acquiring instantaneous CSI is a significant challenge. The analog beamformer in the RF domain suffers from inherent undersampling, while the need to estimate instantaneous CSI for all possible radiation patterns in the EM domain leads to excessive pilot overhead. Moreover, the real-time computation of beamforming matrices across all three domains imposes high computational complexity, severely impacting system processing efficiency. To address these issues, we propose an innovative tri-timescale framework tailored for tri-hybrid beamforming design. This framework decomposes the original non-convex optimization problem in (16) into three independent subproblems, each solvable at a different timescale. This decomposition significantly reduces pilot overhead, enhances computational tractability, and improves overall system efficiency.

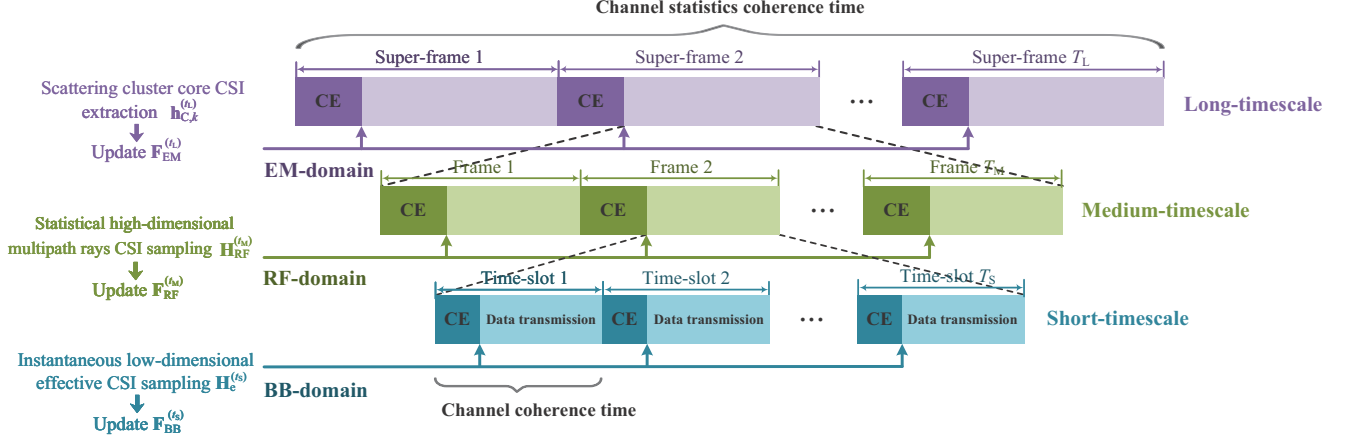


Fig. 4. The frame structure of tri-timescale tri-hybrid beamforming.

III. TRI-TIMESCALE BEAMFORMING DESIGNS

A. Tri-timescale Framework

The tri-hybrid beamforming architecture presents significant practical challenges, including high channel estimation overhead and computational complexity. Estimating the full CSI and jointly optimizing beamformers across all three domains in every time-slot is computationally infeasible. To address this, we propose a tri-timescale beamforming framework that effectively balances practical feasibility and system performance, as illustrated in Fig. 4.

The overall time domain corresponds to the channel statistics coherence time, during which the statistical distribution of the channel remains stable. This period is structured hierarchically, with beamforming operations executed across three distinct timescales, as detailed below:

- **Long-timescale:** The total duration is divided into T_L super-frames, denoted as $\mathcal{T}_L \triangleq \{1, 2, \dots, T_L\}$. In each super-frame, the BS extracts high-dimensional channel information of the scattering cluster core to design the radiation beamformer, ensuring radiation pattern alignment in the EM domain.
- **Medium-timescale:** Each super-frame consists of T_M frames, defined as $\mathcal{T}_M \triangleq \{1, 2, \dots, T_M\}$. In each frame, the BS acquires a statistical channel sample of multi-path rays within the scattering clusters to update the analog beamformer, enhancing array gain in the RF domain.
- **Short-timescale:** Each frame is further divided into T_S time-slots, referred to as the channel coherence time, represented as $\mathcal{T}_S \triangleq \{1, 2, \dots, T_S\}$. In each time-slot, the BS obtains an instantaneous low-dimensional effective CSI to refine the digital beamformer, mitigating multi-user interference and accounting for fast channel fluctuations in the BB domain.

This hierarchical framework significantly reduces channel estimation overhead while ensuring efficient beamforming adaptation across different domains and timescales. In the following subsections, we provide a detailed description of the channel estimation processes and beamforming design procedures based on this tri-timescale framework.

B. Long-timescale EM Domain Design

1) *Long-timescale EM domain Channel Estimation:* Given the specific scattering cluster characteristics described in (4), the angles of the multi-path rays within each scattering cluster exhibit only limited fluctuations around the cluster core. This observation implies that real-time radiation patterns adaptation based on instantaneous CSI is unnecessary. Instead, aligning radiation patterns with the nominal angles of scattering clusters is sufficient to maintain robust communication performance, while significantly reducing channel estimation overhead and beamforming design complexity. Therefore, over the long-timescale, our objective is to estimate the nominal angles and average channel gains of the scattering clusters, which serve as the foundation for radiation beamforming optimization.

Specifically, we employ the Capon algorithm to construct the angular power spectrum (APS) based on the channel covariance matrix, enabling precise spatial domain analysis [29]. To illustrate the channel estimation process, we consider the k -th UE as an example. By accumulating spatial-channel samples over the medium-timescale, the average channel covariance matrix at the t_L -th super-frame is given by

$$\mathbf{R}_k^{(t_L)} = \frac{1}{t_L T_M} \sum_{t_1=1}^{t_L} \sum_{t_M=1}^{T_M} \tilde{\mathbf{h}}_{S,k}^{(t)} (\tilde{\mathbf{h}}_{S,k}^{(t)})^H, \quad \forall k, t_L, \quad (17)$$

where $t = (t_1 - 1)T_M + t_M$ is defined for brevity and $\tilde{\mathbf{h}}_{S,k}$ represents the estimated channel excluding the influence of the radiation patterns, given by

$$\tilde{\mathbf{h}}_{S,k} = \sum_{l=1}^L \alpha_{k,l} \mathbf{a}_{k,l}, \quad \forall k. \quad (18)$$

Then, the APS can be derived as

$$\rho_k^{(t_L)}(\theta) = \frac{1}{\mathbf{e}^H(\theta) (\mathbf{R}_k^{(t_L)})^{-1} \mathbf{e}(\theta)}, \quad \forall k, t_L, \quad (19)$$

with

$$\mathbf{e}(\theta) \triangleq [1, e^{-j\frac{2\pi}{\lambda} d \sin \theta}, \dots, e^{-j\frac{2\pi}{\lambda} (N_t-1) d \sin \theta}]^T \in \mathbb{C}^{N_t}. \quad (20)$$

Since the APS reflects the power distribution across the

angular domain, each peak in the APS physically represents the presence of a distinct scattering cluster in the propagation environment. Thus, the number of the peaks in $\rho_k^{(t_L)}(\theta)$ that exceed a specified threshold directly provides the estimated number of scattering clusters C . For each of these peaks, the corresponding angle value and power value indicate the estimated nominal angle $\bar{\theta}_{k,c}$ and the average channel gain $\alpha_{k,c}$ of the corresponding scattering cluster, respectively. In conclusion, referring to (12), we can construct the EM domain channel, which serves as the foundation for the long-timescale EM domain radiation beamformer design, which yields

$$\mathbf{h}_{C,k} = \bar{\mathbf{H}}_{EM,k} \bar{\mathbf{h}}_{S,k} \in \mathbb{C}^{MN_t}, \quad (21)$$

where the term $\bar{\mathbf{h}}_{S,k} \in \mathbb{C}^{CN_t}$ encapsulates the spatial domain channel characteristics of C scattering cluster cores and $\bar{\mathbf{H}}_{EM,k} \in \{0, 1\}^{MN_t \times CN_t}$ indicates the angle information of the scattering clusters.

2) *Long-timescale Radiation Beamformer Design:* Notably, over the long-timescale, the EM domain radiation beamformer \mathbf{F}_{EM} mainly aims to establish a basic pattern alignment with the scattering cluster core. This optimization requires only the channel information of the scattering cluster core, i.e., the estimated nominal angles and average channel gains of the scattering clusters. Consequently, we substitute the instantaneous multi-path channel \mathbf{h}_k in the SINR expression (14) and the sum-rate formulation (15) with the scattering cluster core channel $\mathbf{h}_{C,k}$, defining the long-timescale sum-rate \bar{R}_k as our optimization objective. Given a fixed analog beamformer \mathbf{F}_{RF} and digital beamformer \mathbf{F}_{BB} , the long-timescale EM domain radiation beamforming design problem is then formulated as

$$\max_{\mathbf{F}_{EM}} \sum_{k=1}^K \bar{R}_k \quad (22a)$$

$$\text{s.t. } \|\mathbf{f}_{EM,n}\|^2 = 1, \quad \forall n. \quad (22b)$$

Considering the hardware implementability of pixel-based pattern-reconfigurable antennas, we adopt a practical approach by selecting the optimal radiation pattern from a predefined set, rather than designing arbitrary patterns with unrestricted directions and shapes. This approach ensures a balance between implementation efficiency and real-world hardware constraints. To be specific, the EM domain radiation beamformer is formulated as

$$\mathbf{F}_{EM} \triangleq \bar{\mathbf{F}}_{\text{pat}} \mathbf{S}_{EM}, \quad (23)$$

where $\bar{\mathbf{F}}_{\text{pat}} \triangleq \mathbf{I}_{N_t} \otimes \mathbf{F}_{\text{pat}} \in \mathbb{R}^{MN_t \times PN_t}$ with $\mathbf{F}_{\text{pat}} \in \mathbb{R}^{M \times P}$ representing a predefined radiation pattern dictionary that contains the radiation gains of P candidate patterns over M spatial sampling angles. The matrix $\mathbf{S}_{EM} \triangleq \text{blkdiag}\{\mathbf{s}_{EM,1}, \mathbf{s}_{EM,2}, \dots, \mathbf{s}_{EM,N_t}\} \in \{0, 1\}^{PN_t \times N_t}$ denotes the EM domain pattern selection matrix, where each $\mathbf{s}_{EM,n} \in \{0, 1\}^P$ selects a single optimal pattern from the dictionary for the n -th antenna, i.e., $\|\mathbf{s}_{EM,n}\|_1 = 1$. Based on this formulation, the original problem in (22) is equivalently transformed into a more practical optimization problem focused on optimizing the EM-domain pattern selection matrix \mathbf{S}_{EM} ,

given by

$$\max_{\mathbf{S}_{EM}} \sum_{k=1}^K \bar{R}_k \quad (24a)$$

$$\text{s.t. } \mathbf{s}_{EM,n}(p) \in \{0, 1\}, \quad \forall n, p, \quad (24b)$$

$$\|\mathbf{s}_{EM,n}\|_1 = 1, \quad \forall n. \quad (24c)$$

The non-convex optimization problem in (24) poses significant challenges due to the fractional and logarithmic terms in the objective function (24a), as well as the non-smooth, non-convex Boolean constraint in (24b). To address these difficulties, we first apply the fractional programming (FP) method to reformulate the objective function (24a) into a polynomial expression, making it more tractable. Subsequently, we transform the Boolean constraint (24b) into a quadratic penalty term with a box constraint and leverage the majorization-minimization (MM) method to facilitate efficient optimization.

Firstly, by employing the Lagrangian dual reformulation and introducing auxiliary variable $\boldsymbol{\mu} \triangleq [\mu_1, \mu_2, \dots, \mu_K]^T$, the objective function (24) can be transformed to

$$\sum_{k=1}^K \log_2(1 + \mu_k) - \sum_{k=1}^K \mu_k + \sum_{k=1}^K \frac{(1 + \mu_k) |\mathbf{h}_{C,k}^H \mathbf{F}_{EM} \mathbf{F}_{RF} \mathbf{f}_{BB,k}|^2}{\sum_{j=1}^K |\mathbf{h}_{C,k}^H \mathbf{F}_{EM} \mathbf{F}_{RF} \mathbf{f}_{BB,j}|^2 + \sigma_k^2}, \quad (25)$$

which is equivalent to the original objective function (24a) when the auxiliary variable $\boldsymbol{\mu}$ has the optimal value

$$\mu_k = \frac{|\mathbf{h}_{C,k}^H \mathbf{F}_{EM} \mathbf{F}_{RF} \mathbf{f}_{BB,k}|^2}{\sum_{j=1, j \neq k}^K |\mathbf{h}_{C,k}^H \mathbf{F}_{EM} \mathbf{F}_{RF} \mathbf{f}_{BB,j}|^2 + \sigma_k^2}, \quad \forall k. \quad (26)$$

However, the summation of fractional terms in (25) still hinders a straightforward solution. Thus, we further adopt the quadratic transform to convert it into

$$2\sqrt{1 + \mu_k} \Re\{\xi_k^* \mathbf{h}_{C,k}^H \mathbf{F}_{EM} \mathbf{F}_{RF} \mathbf{f}_{BB,k}\} - |\xi_k|^2 D_k, \quad \forall k, \quad (27)$$

where $\boldsymbol{\xi} \triangleq [\xi_1, \xi_2, \dots, \xi_K]^T$ is the auxiliary variable and $D_k \triangleq \sum_{j=1}^K |\mathbf{h}_{C,k}^H \mathbf{F}_{EM} \mathbf{F}_{RF} \mathbf{f}_{BB,j}|^2 + \sigma_k^2$ is utilized to simplify the expression. The expression (27) is equivalent to the last fractional term in (25) when the auxiliary variable $\boldsymbol{\xi}$ has the optimal value

$$\xi_k = \frac{\sqrt{1 + \mu_k} \mathbf{h}_{C,k}^H \mathbf{F}_{EM} \mathbf{F}_{RF} \mathbf{f}_{BB,k}}{D_k}, \quad \forall k. \quad (28)$$

Based on the above derivation, the objective function can be reformulated as

$$\sum_{k=1}^K [\log_2(1 + \mu_k) - \mu_k + 2\sqrt{1 + \mu_k} \Re\{\xi_k^* \mathbf{h}_{C,k}^H \mathbf{F}_{EM} \mathbf{F}_{RF} \mathbf{f}_{BB,k}\} - |\xi_k|^2 D_k]. \quad (29)$$

In order to facilitate the subsequent transformation, (29) can be rewritten as the following concise form

$$\sum_{k=1}^K [\log_2(1 + \mu_k) - \mu_k - |\xi_k|^2 \sigma_k^2] + \delta, \quad (30)$$

where we define

$$\delta \triangleq \sum_{k=1}^K \left[2\sqrt{1 + \mu_k} \Re\{\xi_k^* \mathbf{h}_{C,k}^H \mathbf{F}_{EM} \mathbf{F}_{RF} \mathbf{f}_{BB,k}\} - |\xi_k|^2 \sum_{j=1}^K |\mathbf{h}_{C,k}^H \mathbf{F}_{EM} \mathbf{F}_{RF} \mathbf{f}_{BB,j}|^2 \right]. \quad (31)$$

Having the optimal auxiliary variables $\boldsymbol{\mu}$ and $\boldsymbol{\xi}$, maximizing (30) is equivalent to maximizing the term δ . Consequently, we can recast the optimization problem as

$$\max_{\mathbf{S}_{EM}} \delta \quad (32a)$$

$$\text{s.t. } \mathbf{s}_{EM,n}(p) \in \{0, 1\}, \forall n, p, \quad (32b)$$

$$\|\mathbf{s}_{EM,n}\|_1 = 1, \forall n. \quad (32c)$$

After dealing with the objective function, we turn to tackle the neither smooth nor convex Boolean constraint (32b). As stated in [30], the Boolean constraint (32b) can be transformed into an optimization problem of maximizing a quadratic term with a box constraint, which yields

$$\max_{\mathbf{S}_{EM}} \mathbf{s}_{EM}^T (\mathbf{S}_{EM} - \mathbf{1}) \quad (33a)$$

$$\text{s.t. } \mathbf{s}_{EM,n}(p) \in [0, 1], \forall n, p, \quad (33b)$$

where $\mathbf{s}_{EM} \triangleq [\mathbf{s}_{EM,1}^T, \mathbf{s}_{EM,2}^T, \dots, \mathbf{s}_{EM,N_t}^T]^T \in \mathbb{R}^{P N_t}$ is introduced for brevity and the binary variable \mathbf{S}_{EM} has been relaxed to be continuous. Then, we can incorporate the objective function (33a) as a penalty term into the problem (32) with a box constraint (33b), which is given by

$$\max_{\mathbf{S}_{EM}} \delta + \varrho_1 \mathbf{s}_{EM}^T (\mathbf{S}_{EM} - \mathbf{1}) \quad (34a)$$

$$\text{s.t. } \mathbf{s}_{EM,n}(p) \in [0, 1], \forall n, p, \quad (34b)$$

$$\|\mathbf{s}_{EM,n}\|_1 = 1, \forall n, \quad (34c)$$

where ϱ_1 is the penalty parameter. The newly constructed objective function (34a) contains a non-concave quadratic term related to the variable \mathbf{S}_{EM} . Hence, we employ the MM approach in [31] to convert it into a linear form at the current point $\mathbf{s}_{EM}^{(q)}$ in the q -th iteration, which can be expressed as

$$\mathbf{s}_{EM}^T (\mathbf{S}_{EM} - \mathbf{1}) \geq 2(\mathbf{s}_{EM}^{(q)})^T \mathbf{S}_{EM} - (\mathbf{s}_{EM}^{(q)})^T \mathbf{s}_{EM}^{(q)} - \mathbf{s}_{EM}^T \mathbf{1}. \quad (35)$$

Finally, the optimization problem for designing the EM domain pattern selection matrix is formulated as

$$\max_{\mathbf{S}_{EM}} \delta + \varrho_1 (2\mathbf{s}_{EM}^{(q)} - \mathbf{1})^T \mathbf{S}_{EM} \quad (36a)$$

$$\text{s.t. } \mathbf{s}_{EM,n}(p) \in [0, 1], \forall n, p, \quad (36b)$$

$$\|\mathbf{s}_{EM,n}\|_1 = 1, \forall n, \quad (36c)$$

which is convex and can be easily tackled by off-the-shelf solver CVX. With the optimal EM domain pattern selection matrix \mathbf{S}_{EM} and the known radiation pattern dictionary $\bar{\mathbf{F}}_{\text{pat}}$, the radiation beamformer is constructed as $\mathbf{F}_{EM} \triangleq \bar{\mathbf{F}}_{\text{pat}} \mathbf{S}_{EM}$ in (23).

C. Medium-timescale RF Domain Design

1) *Medium-timescale RF Domain Channel Estimation:* The presence of reconfigurable antennas inherently couples the

spatial-domain channel with the radiation pattern gains, as characterized in (12). Conventional channel estimation techniques designed for hybrid architectures do not account for this coupling, leading to estimation inaccuracies due to the neglect of radiation pattern effects on the measured channel [32], [33]. To address this limitation, it is essential to refine traditional estimation methods. Leveraging the inherent sparsity of the scattering cluster channel, we employ a compressed sensing (CS) algorithm for efficient channel estimation. Specifically, we construct a revised dictionary matrix that explicitly incorporates the impact of pattern-reconfigurable antennas, enabling a more accurate representation of the spatial-domain channel characteristics. This enhancement not only improves channel estimation accuracy but also facilitates a more robust and adaptive beamforming strategy, ultimately enhancing overall system performance.

Initially, the RF domain channel to be estimated is expressed as

$$\mathbf{h}_{RF,k} \triangleq \mathbf{F}_{EM}^H \bar{\mathbf{H}}_{EM,k} \bar{\mathbf{h}}_{S,k}, \forall k, \quad (37)$$

where $\mathbf{F}_{EM}^H \bar{\mathbf{H}}_{EM,k}$ reflects the radiation gains of the reconfigurable antennas based on the fixed radiation beamformer determined in the long-timescale, and it is apparent that this term is coupled with the spatial channel $\bar{\mathbf{h}}_{S,k}$. During the training phase, all UEs simultaneously transmit pilot signals on distinct frequency tones to the BS in the uplink. Taking the k -th UE as an example, the received signal at the BS is given by

$$\begin{aligned} \mathbf{y}_k &= \sqrt{P_t} \mathbf{W}_k^H \mathbf{h}_{RF,k} + \mathbf{W}_k^H \mathbf{n}_k \\ &= \sqrt{P_t} \mathbf{W}_k^H \mathbf{A}_D \mathbf{z}_k + \mathbf{W}_k^H \mathbf{n}_k \\ &= \mathbf{Q}_k \mathbf{z}_k + \mathbf{W}_k^H \mathbf{n}_k, \forall k, \end{aligned} \quad (38)$$

where $\mathbf{W}_k \in \mathbb{C}^{N_t \times N_{\text{Beam}}}$ is the training beamformer with N_{Beam} denoting the number of training beams, $\mathbf{A}_D \in \mathbb{C}^{N_t \times M}$ is the refined dictionary matrix incorporating the effects of pattern-reconfigurable antennas, \mathbf{z}_k is a sparse vector with non-zero elements corresponding to the spatial angles, and $\mathbf{Q}_k \triangleq \sqrt{P_t} \mathbf{W}_k^H \mathbf{A}_D$ is the sensing matrix.

The conventional dictionary matrix consists of a set of steering vectors corresponding to uniformly distributed candidate angles, given by

$$\mathbf{E} = [\mathbf{e}(\theta_1), \mathbf{e}(\theta_2), \dots, \mathbf{e}(\theta_M)] \in \mathbb{C}^{N_t \times M}, \quad (39)$$

where each column $\mathbf{e}(\theta_m)$ represents a steering vector pointing toward the angle $\theta_m = \pi m/M$, $m = 1, 2, \dots, M$. To explicitly account for the influence of the reconfigurable antenna pattern on the channel representation, we refine the dictionary matrix as

$$\mathbf{A}_D(:, m) = \mathbf{F}_{EM}(:, m) \odot \mathbf{e}(\theta_m), \forall m, \quad (40)$$

where $\mathbf{F}_{EM}(:, m)$ characterizes the radiation gains of the N_t antennas in the direction of θ_m . This formulation effectively integrates both radiation pattern effects and angular information, enabling a more accurate estimation of spatial channel characteristics.

Subsequently, the channel estimation problem can be for-

mulated as a sparse recovery problem:

$$\min_{\mathbf{z}_k} \|\mathbf{y}_k - \mathbf{Q}_k \mathbf{z}_k\|_2 \quad (41a)$$

$$\text{s.t.} \quad \|\mathbf{z}_k\|_0 = L. \quad (41b)$$

This problem is typically solved using the orthogonal matching pursuit (OMP) algorithm, which iteratively selects the most relevant dictionary elements to approximate the signal. The iterations continue until the residual error falls below a predefined threshold or the sparsity constraint is met. The implementation details of the OMP algorithm and the design of the training hybrid beamformer follow the principles outlined in [32], [33]. For brevity, these details are omitted here.

2) *Medium-timescale Analog Beamformer Design:* With the radiation beamformer \mathbf{F}_{EM} determined in the long-timescale, we now focus on designing the analog beamformer in the medium-timescale based on the statistical CSI of multipath rays. Given the statistical information of the channel, the objective function is adjusted to maximize the ergodic sum-rate, ensuring robust performance over average channel conditions. Thus, the analog beamformer design problem in the medium-timescale is formulated as follows

$$\max_{\mathbf{F}_{\text{RF}}} \sum_{k=1}^K \tilde{R}_k \quad (42a)$$

$$\text{s.t.} \quad \mathbf{F}_{\text{RF}}(n, l_{\text{RF}}) \in \{\mathcal{F}, 0\}, \quad \forall n, l_{\text{RF}}, \quad (42b)$$

$$\|\mathbf{F}_{\text{RF}}(n, :)\|_0 = 1, \quad \forall n, \quad (42c)$$

where (42a) defines the ergodic sum-rate $\tilde{R}_k \triangleq \mathbb{E}_{\mathbf{H}_{\text{RF}}} \{R_k\}$, evaluated over the RF domain channel samples, denoted as $\mathbf{H}_{\text{RF}} \triangleq [\mathbf{h}_{\text{RF},1}, \mathbf{h}_{\text{RF},2}, \dots, \mathbf{h}_{\text{RF},K}] \in \mathbb{C}^{N_t \times K}$ with $\mathbf{h}_{\text{RF},k}$ given in (37). Notably, in this RF domain analog beamformer design problem, the power constraint is not explicitly imposed since the digital beamformer can be subsequently adjusted to satisfy it.

Unlike conventional statistical CSI-based beamforming approaches that require explicit knowledge of the channel statistics, we adopt an online learning framework that incrementally updates the channel statistical information by observing one channel sample at a time. This learning-based approach significantly reduces measurement overhead and latency, making it particularly well-suited for the tri-hybrid beamforming architecture. However, solving (42) is challenging due to the combination of discrete phase constraints in (42b) and the sparsity constraint in (42c), which collectively impose a highly non-convex set for \mathbf{F}_{RF} . To overcome these challenges, we decompose the analog beamformer into two components:

$$\mathbf{F}_{\text{RF}} \triangleq \mathbf{S}_{\text{RF}} \mathbf{F}_{\text{set}}, \quad (43)$$

where $\mathbf{S}_{\text{RF}} \in \{0, 1\}^{N_t \times N_{\text{RF}} 2^B}$ is the RF domain phase-shift selection matrix and \mathbf{F}_{set} is defined as $\mathbf{F}_{\text{set}} \triangleq \mathbf{I}_{N_{\text{RF}}} \otimes \mathbf{f}_{\text{set}}$ with

$$\mathbf{f}_{\text{set}} \triangleq \frac{1}{\sqrt{N_t}} \left[1, e^{-j\frac{2\pi}{2^B}}, \dots, e^{-j\frac{2\pi(2^B-1)}{2^B}} \right]^T, \quad (44)$$

containing all possible phase-shifts for a low-resolution PS. The binary matrix \mathbf{S}_{RF} encodes phase-shift selections, where $\mathbf{S}_{\text{RF}}(n, l_{\text{RF}}) = 1$ indicates that the n -th antenna is assigned

to the $l_{\text{RF}}/2^B$ -th RF chain with the corresponding phase-shift value given by $\mathbf{F}_{\text{set}}(l_{\text{RF}}, l_{\text{RF}}/2^B)$. With \mathbf{F}_{set} predefined, the analog beamformer design problem (42) can be equivalently formulated as

$$\max_{\mathbf{S}_{\text{RF}}} \sum_{k=1}^K \tilde{R}_k \quad (45a)$$

$$\text{s.t.} \quad \mathbf{S}_{\text{RF}}(n, l_{\text{RF}}) \in \{0, 1\}, \quad \forall n, l_{\text{RF}}, \quad (45b)$$

$$\|\mathbf{S}_{\text{RF}}(n, :)\|_1 = 1, \quad \forall n, \quad (45c)$$

where the sum-rate expression in (45a) can be recast as

$$\tilde{R}_k = \log\left(1 + \frac{|\mathbf{h}_{\text{RF},k}^H \mathbf{S}_{\text{RF}} \mathbf{F}_{\text{set}} \mathbf{f}_{\text{BB},k}|^2}{\sum_{j=1, j \neq k}^K |\mathbf{h}_{\text{RF},k}^H \mathbf{S}_{\text{RF}} \mathbf{F}_{\text{set}} \mathbf{f}_{\text{BB},j}|^2 + \sigma_k^2}\right), \quad \forall k. \quad (46)$$

The primary challenges in solving this problem stem from the stochastic nature of the objective function (45a), which lacks a closed-form expression, and the non-smooth, non-convex Boolean constraint (45b). To address these issues, we employ a stochastic successive convex approximation (SSCA) framework [25], which iteratively refines the beamformer based on observed channel realizations. The expectation in the objective function is approximated using a quadratic surrogate function, allowing for online adaptation without requiring explicit statistical knowledge of the channel. Furthermore, the Boolean constraint is handled using a penalty-based approach, similar to the method described in Section III-B.

First, we construct a recursive quadratic surrogate function for the objective function (45a), leveraging both current and past channel samples. This iterative approach enables the BS to gradually learn the statistical properties of the channel by continuously accumulating channel observations, thereby enhancing beamforming performance over time and ensuring convergence. For convenience in the following expressions, we define $g_0(\mathbf{s}_{\text{RF}}; \mathbf{H}_{\text{RF}}) \triangleq R_k$, and introduce $\mathbf{s}_{\text{RF}} \triangleq \text{vec}(\mathbf{S}_{\text{RF}})$.

At the t_M -th recursion, based on the acquired channel sample $\mathbf{H}_{\text{RF}}^{(t_M)}$ and the previous analog beamformer $\mathbf{s}_{\text{RF}}^{(t_M)}$, we can substitute (45a) with a quadratic surrogate function as follows

$$f^{(t_M)}(\mathbf{s}_{\text{RF}}) = v_{\text{SRF}}^{(t_M)} + (\mathbf{v}_{\text{SRF}}^{(t_M)})^T (\mathbf{s}_{\text{RF}} - \mathbf{s}_{\text{RF}}^{(t_M)}) - \tau \|\mathbf{s}_{\text{RF}} - \mathbf{s}_{\text{RF}}^{(t_M)}\|^2, \quad (47)$$

where $\tau > 0$ is a constant ensuring strong convexity of $\tau \|\mathbf{s}_{\text{RF}} - \mathbf{s}_{\text{RF}}^{(t_M)}\|^2$. The term $v_{\text{SRF}}^{(t_M)}$ serves as an approximation of the objective function value $\mathbb{E}_{\mathbf{H}_{\text{RF}}} \{g_0(\mathbf{s}_{\text{RF}}; \mathbf{H}_{\text{RF}})\}$, which is updated recursively as

$$v_{\text{SRF}}^{(t_M)} = (1 - \eta^{(t_M)}) v_{\text{SRF}}^{(t_M-1)} + \eta^{(t_M)} g_0(\mathbf{s}_{\text{RF}}^{(t_M)}; \mathbf{H}_{\text{RF}}^{(t_M)}), \quad (48)$$

where $\eta^{(t_M)} \in (0, 1]$ is a properly chosen sequence to satisfy convergence requirements. Similarly, the gradient term $\mathbf{v}_{\text{SRF}}^{(t_M)}$ is an approximation of the partial derivative of $\mathbb{E}_{\mathbf{H}_{\text{RF}}} \{g_0(\mathbf{s}_{\text{RF}}; \mathbf{H}_{\text{RF}})\}$ with respect to \mathbf{s}_{RF} , evaluated at $\mathbf{s}_{\text{RF}} = \mathbf{s}_{\text{RF}}^{(t_M)}$. This is recursively computed as

$$\mathbf{v}_{\text{SRF}}^{(t_M)} = (1 - \eta^{(t_M)}) \mathbf{v}_{\text{SRF}}^{(t_M-1)} + \eta^{(t_M)} \nabla_{\mathbf{s}_{\text{RF}}} g_0(\mathbf{s}_{\text{RF}}^{(t_M)}; \mathbf{H}_{\text{RF}}^{(t_M)}). \quad (49)$$

The gradient of $g_0(\mathbf{s}_{\text{RF}}; \mathbf{H}_{\text{RF}})$ with respect to \mathbf{s}_{RF} is given by

$$\nabla_{\mathbf{s}_{\text{RF}}} g_0(\mathbf{s}_{\text{RF}}; \mathbf{H}_{\text{RF}}) = \sum_{k=1}^K \left(\frac{\sum_i^K \mathbf{e}_{k,i}}{\Gamma_k} - \frac{\sum_{i \neq k}^K \mathbf{e}_{k,i}}{\Gamma_{-k}} \right), \quad (50)$$

where we define

$$\Gamma_k = \sum_i^K |\mathbf{h}_{\text{RF},k}^H \mathbf{S}_{\text{RF}} \mathbf{F}_{\text{set}} \mathbf{f}_{\text{BB},i}|^2 + \sigma_k^2, \quad \forall k, \quad (51a)$$

$$\Gamma_{-k} = \sum_{i \neq k}^K |\mathbf{h}_{\text{RF},k}^H \mathbf{S}_{\text{RF}} \mathbf{F}_{\text{set}} \mathbf{f}_{\text{BB},i}|^2 + \sigma_k^2, \quad \forall k, \quad (51b)$$

$$\mathbf{e}_{k,i} = 2\Re\{\text{vec}((\mathbf{h}_{\text{RF},k} \mathbf{h}_{\text{RF},k}^H) \mathbf{S}_{\text{RF}} (\mathbf{F}_{\text{set}} \mathbf{f}_{\text{BB},i} \mathbf{f}_{\text{BB},i}^H \mathbf{F}_{\text{set}}^H))\}. \quad (51c)$$

Due to space limitations, we omit the detailed derivations here. The surrogate function $f^{(t_M)}(\mathbf{s}_{\text{RF}})$ in (47) provides a concave approximation of the original stochastic objective function $\mathbb{E}_{\mathbf{H}_{\text{RF}}}\{g_0(\mathbf{s}_{\text{RF}}; \mathbf{H}_{\text{RF}})\}$ in (45a), enabling efficient processing of problem (45) without explicitly computing the expectation.

To deal with the Boolean constraint (45b), we employ the same technique as specified in (33)-(35). As a result, the analog beamformer design problem is formulated as

$$\max_{\mathbf{S}_{\text{RF}}} f^{(t_M)}(\mathbf{s}_{\text{RF}}) + \varrho_2 (2\mathbf{S}_{\text{RF}}^{(t_M)} - \mathbf{1})^T \mathbf{s}_{\text{RF}} \quad (52a)$$

$$\text{s.t. } \mathbf{S}_{\text{RF}}(n, l_{\text{RFB}}) \in [0, 1], \quad \forall n, l_{\text{RFB}}, \quad (52b)$$

$$\|\mathbf{S}_{\text{RF}}(n, :)\|_1 = 1, \quad \forall n, \quad (52c)$$

in which ϱ_2 denotes the penalty parameter. The resulting problem can be efficiently solved using a variety of existing methods or convex optimization solvers. Once the optimal solution, denoted as $\bar{\mathbf{S}}_{\text{RF}}^{(t_M)}$, is obtained, the phase-shift selection matrix \mathbf{S}_{RF} is updated to incorporate both the newly computed solution and the previous information. This update is performed using the following recursive expression:

$$\mathbf{S}_{\text{RF}}^{(t_M+1)} = (1 - \eta^{(t_M)}) \mathbf{S}_{\text{RF}}^{(t_M)} + \eta^{(t_M)} \bar{\mathbf{S}}_{\text{RF}}^{(t_M)}. \quad (53)$$

With the updated phase-shift selection matrix $\mathbf{S}_{\text{RF}}^{(t_M+1)}$, the analog beamformer is then constructed as $\mathbf{F}_{\text{RF}}^{(t_M+1)} = \mathbf{S}_{\text{RF}}^{(t_M+1)} \mathbf{F}_{\text{set}}$.

D. Short-timescale Digital Beamformer Design

In the t_S -th short time-slot of the t_M -th frame, the digital beamformer is updated while keeping the radiation beamformer \mathbf{F}_{EM} and the analog beamformer \mathbf{F}_{RF} fixed. The update relies on the instantaneous low-dimensional effective CSI, denoted as $\mathbf{H}_e^{(t_S)} = (\mathbf{H}_{\text{RF}}^{(t_S)})^H \mathbf{F}_{\text{RF}}^{(t_M)} \in \mathbb{C}^{K \times N_{\text{RF}}}$, which is obtained from the processing of pilot signals in the BB domain. To design the digital beamformer, we apply the classic minimum mean square error (MMSE) method. The resulting digital beamformer is given by

$$\tilde{\mathbf{F}}_{\text{BB}}^{(t_S)} = (\mathbf{H}_e^{(t_S)})^H \left(\mathbf{H}_e^{(t_S)} (\mathbf{H}_e^{(t_S)})^H + \sigma_k^2 \mathbf{I}_K \right)^{-1}. \quad (54)$$

Finally, to ensure compliance with the total power constraint, the digital beamformer is normalized as

$$\mathbf{F}_{\text{BB}}^{(t_S)} = \frac{\sqrt{P_t} \tilde{\mathbf{F}}_{\text{BB}}^{(t_S)}}{\|\mathbf{F}_{\text{RF}}^{(t_M)} \tilde{\mathbf{F}}_{\text{BB}}^{(t_S)}\|_F}. \quad (55)$$

Algorithm 1 The proposed tri-timescale tri-hybrid beamforming design algorithm.

Initialize $\mathbf{F}_{\text{EM}}, \mathbf{F}_{\text{RF}}, \mathbf{F}_{\text{BB}}$.

Step 1: Long-timescale EM domain design at the t_L -th super-frame

- High-dimensional scattering cluster core channel estimation
 - Calculate the channel covariance matrix $\mathbf{R}_k^{(t_L)}, \forall k$ by (17).
 - Derive the APS $\rho_k^{(t_L)}(\theta), \forall k$ as (19).
 - Estimate the nominal angles $\theta_{k,c}, \forall k, c$, and average channel gains $\alpha_{k,c}, \forall k, c$, of the scattering clusters.
 - Construct the EM domain channel $\mathbf{h}_{C,k}^{(t_L)}$ by (21).
- Radiation beamformer design
 - Calculate EM domain pattern selection matrix \mathbf{S}_{EM} .
 - while** no convergence of \mathbf{S}_{EM} **do**
 - Update $\boldsymbol{\mu}$ by (26).
 - Update $\boldsymbol{\xi}$ by (28).
 - Update pattern selection matrix \mathbf{S}_{EM} by solving (36).
 - end while**
 - Construct the radiation beamformer $\mathbf{F}_{\text{EM}}^{(t_L)}$ by (23).

Step 2: Medium-timescale RF domain design at the t_M -th frame

- Statistical high-dimensional multi-path rays channel estimation
 - Construct the modified dictionary matrix $\mathbf{A}_D^{(t_M)}$ by (40).
 - Solve the channel estimation problem (41) by the OMP algorithm.
 - Construct the RF domain channel $\mathbf{h}_{\text{RF},k}^{(t_M)}, \forall k$, by (37).
- Analog beamformer design
 - Update the surrogate function (47) based on $\mathbf{H}_{\text{RF}}^{(t_M)}, \mathbf{S}_{\text{RF}}^{(t_M)}$.
 - Calculate the optimal $\bar{\mathbf{S}}_{\text{RF}}^{(t_M)}$ using (52).
 - Update $\mathbf{S}_{\text{RF}}^{(t_M+1)}$ according to (53).
 - Construct the analog beamformer $\mathbf{F}_{\text{RF}}^{(t_M+1)}$ by (43).

Step 3: Short-timescale BB domain design at the t_S -th time-slot

- Instantaneous low-dimensional effective channel estimation
 - Observe an instantaneous low-dimensional effective channel sample $\mathbf{H}_e^{(t_S)}$.
 - Digital beamformer design
 - With fixed $\mathbf{F}_{\text{EM}}^{(t_L)}$ and $\mathbf{F}_{\text{RF}}^{(t_M)}$, calculate the digital beamformer $\mathbf{F}_{\text{BB}}^{(t_S)}$ according to (54) and (55).
-

E. Summary, Complexity and Overhead Analysis

1) *Summary*: Based on the above derivations, the proposed tri-timescale tri-hybrid beamforming design is straightforward and summarized in Algorithm 1. After appropriately initializing the beamforming matrices $\mathbf{F}_{\text{EM}}, \mathbf{F}_{\text{RF}}$ and \mathbf{F}_{BB} across the three domains, the algorithm iteratively acquires the corresponding channel information and updates these matrices over the three timescales, respectively.

2) *Complexity Analysis*: Next, we provide a brief analysis of the algorithmic complexity. The primary computational complexity lies in calculating the EM domain pattern selection matrix \mathbf{S}_{EM} in (36) over the long-timescale, and determining the phase-shift selection matrix \mathbf{S}_{RF} in (52) over the medium-timescale. Specifically, the computational complexity of solving problem (36) in each super-frame over the long-timescale, which involves an $N_t P$ -dimensional variable and requires handling $2N_t P$ second-order cone (SOC) constraints, is of order $\mathcal{O}\{\sqrt{2N_t P} + N_t + 1N_t P(N_t^2 P^2 + 2N_t P + N_t)\}$ [34]. Similarly, the computational complexity of solving problem (52) in each frame during the medium-

timescale, which entails calculating an $N_t N_{\text{RF}} 2^B$ -dimensional variable along with $2N_t N_{\text{RF}} 2^B$ SOC constraints, is of order $\mathcal{O}\{\sqrt{2N_t N_{\text{RF}} 2^B + N_t} + 1N_t N_{\text{RF}} 2^B (N_t^2 N_{\text{RF}}^2 2^{2B} + 2N_t N_{\text{RF}} 2^B + N_t)\}$.

3) *Pilot Overhead Analysis*: The pilot overhead in the proposed scheme primarily stems from channel sampling at the medium-timescale and short-timescale stages. In the medium-timescale, CS-based channel estimation requires $N_{\text{Beam}} K / N_{\text{RF}}$ pilot symbols to obtain the RF domain high-dimensional statistical channel sample $\mathbf{h}_{\text{RF},k}^{(t_M)}, \forall k$, as described in Section III-C. In the short-timescale, $N_{\text{RF}} K$ pilot symbols are needed for estimating the BB domain low-dimensional effective channel $\mathbf{H}_e^{(t_S)}$, as described in Section III-D. Therefore, the total pilot overhead across the channel statistics coherence time is expressed as $(N_{\text{Beam}} K / N_{\text{RF}} + N_{\text{RF}} K T_S) T_M T_L$. This is notably less than that of the real-timescale beamforming approaches, which requires $(N_{\text{Beam}} K / N_{\text{RF}} + N_{\text{RF}} K) T_S T_M T_L$.

IV. SIMULATION RESULTS

In this section, we provide simulation results to demonstrate the effectiveness of the proposed tri-timescale tri-hybrid beamforming design algorithm with reconfigurable antennas in enhancing communication performance while ensuring hardware efficiency. Unless otherwise specified, the BS is equipped with $N_t = 32$ antennas and the center carrier frequency is set to $f_c = 28$ GHz. The low-resolution PS used in the RF domain has quantized phase controlled by $B = 3$ bits. Without loss of generality, we assume that the number of UEs K is equal to the number of RF chains N_{RF} . In the EM domain, each pixel-based reconfigurable antenna enables the generation of $P = 7$ distinct directional radiation patterns by adjusting the electronic switches between pixels [8], with $M = 180$ uniform sampling points in the azimuth dimension. In this scenario, there are $K = 2$ UEs, all operating under a scattering cluster channel with $C = 2$ clusters, each of which consists of $L_c = 3$ multi-path rays. The nominal AoDs $\bar{\theta}_{k,c}$ of these scattering clusters are randomly distributed within $[-\pi/3, \pi/3]$, while the angle spread is set to $\zeta_{k,c} = \pi/36$. The path loss is expressed as $\alpha_{k,c,l_c} = 10^{-\frac{C_0}{10} \left(\frac{r_{k,c,l_c}}{D_0} \right)^{-\kappa_{k,c,l_c}}}$ with $\kappa_{k,c,l_c} \in [2.5, 3]$ being the attenuation factor, $C_0 = 30$ dB, $D_0 = 1$ m. The propagation distance r_{k,c,l_c} is composed of the nominal distance $\bar{r}_{k,c} \in [50\text{m}, 100\text{m}]$ and $\iota = 0.5$ m. The noise power of UEs is set as $\sigma_k^2 = -70$ dBm. The tri-timescale framework is structured with $T_L = 10$ super-frames for the long-timescale, $T_M = 50$ frames for the medium-timescale, and $T_S = 200$ time-slots for the short-timescale.

The convergence performance of the proposed tri-timescale tri-hybrid beamforming design is illustrated in Fig. 5, which includes both the long-timescale radiation beamformer design algorithm and the medium-timescale analog beamformer design algorithm. It should be emphasized that the convergence implications differ between the two algorithms. In the long-timescale case, convergence refers to the iterative calculation of the radiation beamformer at the start of super-frame, based on the estimated CSI of the scattering cluster core. In contrast, for the medium-timescale case, the convergence process refers to the recursive learning of the channel statistics of the multi-path rays within the scattering clusters using high-dimensional

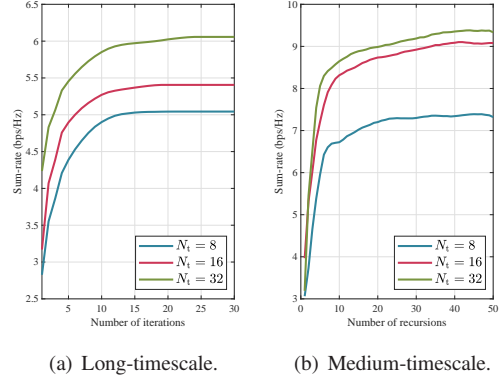


Fig. 5. Convergence performance of the long-timescale radiation beamformer design and medium-timescale analog beamformer design.

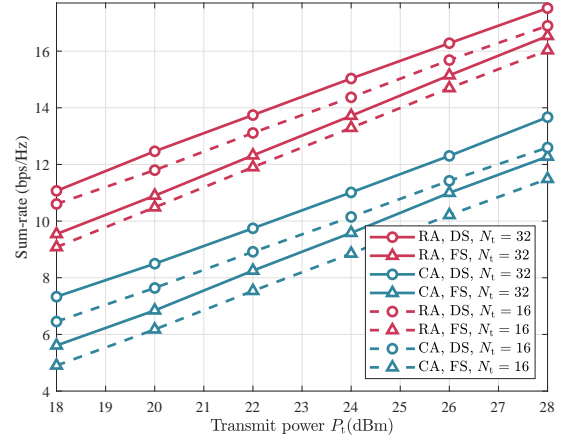


Fig. 6. The sum-rate versus the transmit power P_t .

channel samples and the recursive updating of the analog beamformer in each frame. The results presented in Fig. 5 demonstrate that both algorithms exhibit satisfactory convergence speed, indicating an efficient level of computational complexity.

Fig. 6 illustrates the sum-rate performance versus transmit power for systems employing reconfigurable and conventional antennas. Specifically, the proposed tri-hybrid beamforming architecture with reconfigurable antennas and a dynamic-subarray scheme is denoted as “**RA, DS**”. For comparison, hybrid beamforming using conventional antennas with a dynamic-subarray is labeled “**CA, DS**”, and the fixed-subarray architectures with reconfigurable and conventional antennas are denoted as “**RA, FS**” and “**CA, FS**”, respectively. Performance is evaluated for systems with $N_t = 32$ and $N_t = 16$ antennas. As shown in Fig. 6, the proposed “**RA, DS**” algorithm consistently outperforms its competitors. In particular, reconfigurable antennas yield a power gain of approximately 7 dB compared to conventional antennas, while the dynamic-subarray scheme provides an additional gain of about 2 dB over the fixed-subarray approach. These results confirm that the tri-hybrid beamforming architecture achieves

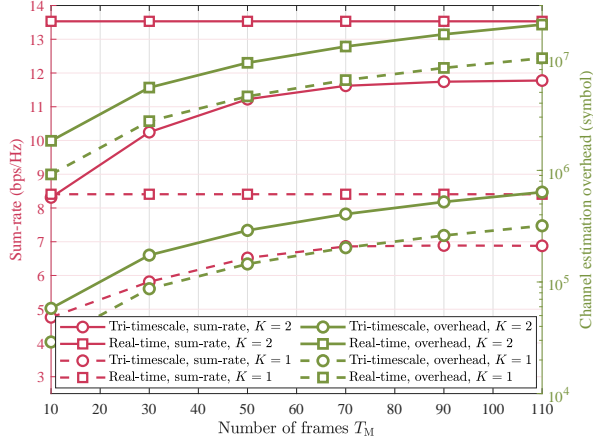


Fig. 7. The sum-rate and channel estimation overhead versus the number of frames T_M .

superior communication performance by virtue of its enhanced flexibility in radiation pattern selection in the EM domain and subarray selection in the RF domain.

For the proposed tri-timescale tri-hybrid beamforming design, increasing the channel sampling rate in the medium-timescale can enhance sum-rate performance by enabling more frequent updates of channel statistics for multi-path rays and scattering cluster cores. However, this improvement comes at the cost of higher pilot overhead. To quantitatively evaluate the impact of the channel sampling rate on both system performance and pilot overhead, we gradually increase the number of frames per super-frame in the medium-timescale, effectively increasing the channel sampling rate, as illustrated in Fig. 7. By analyzing the pilot overhead expression derived in Section III-E and observing the trend in Fig. 7, we conclude that the proposed tri-timescale scheme significantly reduces pilot overhead compared to the real-time scheme, which requires high-dimensional CSI estimation in every time-slot. More importantly, as the number of frames increases, the sum-rate performance of the tri-timescale beamforming scheme steadily improves and eventually saturates at a satisfactory level, albeit with a monotonic increase in channel estimation overhead. In particular, setting the number of frames to $T_M = 50$ achieves a favorable balance between performance and overhead, a configuration adopted in the simulations.

The channel estimation algorithms in both the EM and RF domains are critical components of the proposed tri-timescale framework. Fig. 8 illustrates the impact of different channel estimation configurations on sum-rate performance under various system settings. The results indicate that, regardless of the number of propagation paths L_c , the sum-rate achieved with estimated CSI is highly comparable to that with perfect CSI. This finding underscores the accuracy and robustness of our channel estimation algorithms within the proposed framework, even under complex propagation conditions. Moreover, even with a reduced angular resolution N_{Beam} , the channel characteristics are reliably captured, and acceptable sum-rate performance is achieved, further validating the effectiveness

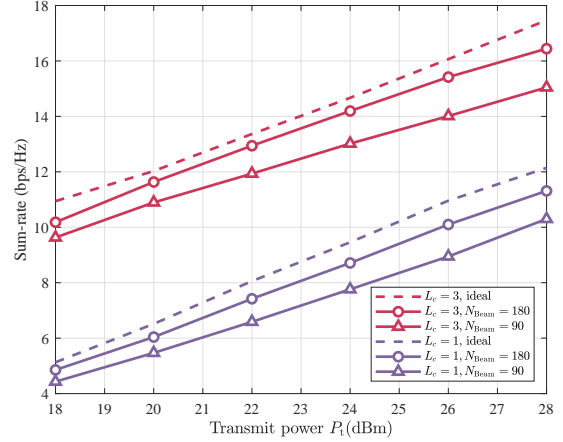


Fig. 8. The impact of channel estimation configurations on sum-rate performance.

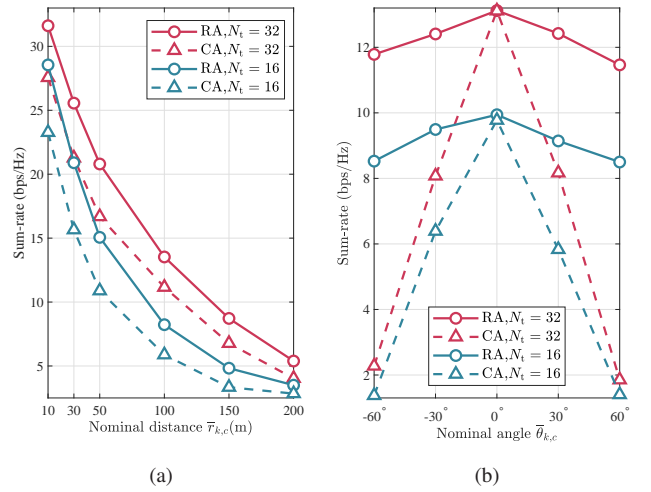


Fig. 9. The sum-rate versus the distance and angle of UE.

and reliability of the proposed approach.

Finally, we validate the effectiveness of the proposed scheme by evaluating the impact of user location on the overall performance of the tri-hybrid beamforming with reconfigurable antennas (RA) and the hybrid beamforming with conventional antennas (CA). Specifically, Fig. 9 (a) depicts the sum-rate performance as a function of the nominal distance, which represents the distance between the BS and the UEs, while Fig. 9 (b) illustrates the sum-rate variation with respect to the nominal angle, which represents the user's angular position relative to the antenna array. From Fig. 9 (a), we observe that as the nominal distance increases, the performance gain offered by pattern-reconfigurable antennas gradually diminishes. This is primarily due to the dominant effect of path loss, which attenuates signal power, reducing the relative impact of radiation pattern variations across different angles. In contrast, Fig. 9 (b) reveals that the RA-based scheme maintains robust performance across a wide range of user angles by dynamically adjusting the pattern orientations

as the user's position deviates from the optimal direction. In comparison, the CA-based scheme achieves satisfactory performance only when the user is positioned perpendicular to the array, where the antenna gain is maximized. These results underscore the robustness and versatility of the proposed tri-hybrid beamforming approach, demonstrating that dynamic pattern reconfiguration not only compensates for variations in user location but also substantially enhances overall system performance and reliability across a wide range of deployment scenarios.

V. CONCLUSIONS

This paper presents a novel tri-hybrid beamforming architecture that integrates pattern-reconfigurable antennas with analog and digital beamforming. By leveraging an innovative tri-timescale beamforming framework, the proposed approach optimizes the radiation beamformer over a long-timescale, the analog beamformer over a medium-timescale, and the digital beamformer over a short-timescale. This hierarchical design effectively balances system performance with practical constraints, such as channel estimation overhead and computational complexity. Extensive simulation results validate the superiority of the proposed scheme over conventional hybrid beamforming architectures, highlighting its potential in future wireless communication systems.

REFERENCES

- [1] W. Saad, M. Bennis, and M. Chen, "A vision of 6G wireless systems: Applications, trends, technologies, and open research problems," *IEEE Network*, vol. 34, no. 3, pp. 134-142, May 2020.
- [2] E. Björnson, L. Sanguinetti, H. Wymeersch, J. Hoydis, and T. L. Marzetta, "Massive MIMO is a reality-what is next?: Five promising research directions for antenna arrays," *Digit. Signal Process.*, vol. 94, pp. 3-20, Nov. 2019.
- [3] C. You, Y. Cai, Y. Liu, M. Di Renzo, T. M. Duman, and A. Yener, "Next generation advanced transceiver technologies for 6G and beyond," *IEEE J. Sel. Areas Commun.*, vol. 43, no. 3, pp. 582-627, Mar. 2025.
- [4] W. K. New *et al.*, "A tutorial on fluid antenna system for 6G networks: Encompassing communication theory, optimization methods and hardware designs," *IEEE Commun. Surveys Tuts.*, early access, Nov. 2024, doi: 10.1109/COMST.2024.3498855.
- [5] T. Wu *et al.*, "Fluid antenna systems enabling 6G: Principles, applications, and research directions," Dec. 2024. [Online]. Available: <https://arxiv.org/abs/2412.03839v1>
- [6] B. He and H. Jafarkhani, "Millimeter wave communications with reconfigurable antennas," in *Proc. IEEE Int. Conf. Commun. (ICC)*, Kansas City, MO, USA, May 2018.
- [7] B. He and H. Jafarkhani, "Low-complexity reconfigurable MIMO for millimeter wave communications," *IEEE Trans. Wireless Commun.*, vol. 66, no. 11, pp. 5278-5291, Jul. 2018.
- [8] Y. Zhang, Z. Han, S. Tang, S. Shen, C.-Y. Chiu, and R. Murch, "A highly pattern-reconfigurable planar antenna with 360° single- and multi-beam steering," *IEEE Trans. Wireless Commun.*, vol. 70, no. 8, pp. 6490-6504, Aug. 2022.
- [9] P. Lotfi, S. Soltani, and R. Murch, "Printed endfire beam-steerable pixel antenna," *IEEE Trans. Antennas Propag.*, vol. 65, no. 8, pp. 3913-3923, Jun. 2017.
- [10] Y. Zhang *et al.*, "A low-profile microstrip vertically polarized endfire antenna with 360° beam-scanning and high beam-shaping capability," *IEEE Trans. Antennas Propag.*, vol. 70, no. 9, pp. 7691-7702, May 2022.
- [11] S. Song and R. Murch, "An efficient approach for optimizing frequency reconfigurable pixel antennas using genetic algorithms," *IEEE Trans. Antennas Propag.*, vol. 62, no. 2, pp. 609-620, Feb. 2014.
- [12] M. R. Castellanos and R. W. Heath, "Linear polarization optimization for wideband MIMO systems with reconfigurable arrays," *IEEE Trans. Wireless Commun.*, vol. 23, no. 3, pp. 2282-2295, Mar. 2024.
- [13] W. Zheng, Y. Yang, and H. Li, "Design of polarization reconfigurable pixel antennas with optimized PIN-diode implementation," *IEEE Trans. Antennas Propag.*, vol. 73, no. 2, pp. 851-862, Oct. 2024.
- [14] C. Zhang, S. Shen, Z. Han, and R. Murch, "Analog beamforming using ESPAR for single-RF precoding systems," *IEEE Trans. Wireless Commun.*, vol. 22, no. 7, pp. 4387-4440, Jul. 2023.
- [15] C. Gu *et al.*, "3-D coverage beam-scanning antenna using feed array and active frequency-selective surface," *IEEE Trans. Antennas Propag.*, vol. 65, no. 11, pp. 5862-5870, Nov. 2017.
- [16] J. Zhang *et al.*, "A novel pixel-based reconfigurable antenna applied in fluid antenna systems with high switching speed," *IEEE Open J. Commun. Soc.*, vol. 6, pp. 212-228, Feb. 2025.
- [17] T. Wu, S. Shen, K.-K. Wong, and R. Murch, "Antenna coding empowered by pixel antennas," Nov. 2024. [Online]. Available: <https://arxiv.org/abs/2411.06642v1>
- [18] K. Ying, Z. Gao, Y. Su, T. Qin, M. Matthaiou, and R. Schober, "Reconfigurable massive MIMO: Precoding design and channel estimation in the electromagnetic domain," *IEEE Trans. Commun.*, early access, Oct. 2024. doi: 10.1109/TCOMM.2024.3485587.
- [19] C. Han, L. Yan, and J. Yuan, "Hybrid beamforming for terahertz wireless communications: Challenges, architectures, and open problems," *IEEE Wireless Commun.*, vol. 28, no. 4, pp. 198-204, Aug. 2021.
- [20] F. Sahrabi and W. Yu, "Hybrid digital and analog beamforming design for large-scale MIMO systems," *IEEE J. Sel. Topics Signal Process.*, vol. 10, no. 3, pp. 501-513, Apr. 2016.
- [21] X. Gao, L. Dai, S. Han, I. Chih-Lin, and R. W. Heath, "Energy-efficient hybrid analog and digital precoding for mmWave MIMO systems with large antenna arrays," *IEEE J. Sel. Areas Commun.*, vol. 34, no. 4, pp. 998-1009, Apr. 2016.
- [22] H. Li, M. Li, Q. Liu, and A. L. Swindlehurst, "Dynamic hybrid beamforming with low-resolution PSs for wideband mmWave MIMO-OFDM systems," *IEEE J. Sel. Areas Commun.*, vol. 38, no. 9, pp. 2168-2181, Sep. 2020.
- [23] M. R. Castellanos, J. Carlson, and R. W. Heath, "Energy-efficient tri-hybrid precoding with dynamic metasurface antennas" in *Asilomar Conf. on Signals, Systems, and Computers*, Pacific Grove, CA, USA, Oct. 2023.
- [24] M. R. Castellanos, S. Yang, C.-B. Chae, and R. W. Heath, "Embracing reconfigurable antennas in the tri-hybrid MIMO architecture for 6G," Jan. 2025. [Online]. Available: <https://arxiv.org/abs/2501.16610v1>
- [25] A. Liu, V. K. N. Lau, and M.-J. Zhao, "Online successive convex approximation for two-stage stochastic nonconvex optimization," *IEEE Trans. Signal Process.*, vol. 66, no. 22, pp. 5941-5955, Nov. 2018.
- [26] Y. Cai, K. Xu, A. Liu, M. Zhao, B. Champagne, and L. Hanzo, "Two-timescale hybrid analog-digital beamforming for mmWave full-duplex MIMO multiple-relay aided systems," *IEEE J. Sel. Areas Commun.*, vol. 38, no. 9, pp. 2086-2103, Sep. 2020.
- [27] Y. Teng, Y. Zhao, M. Wei, A. Liu, and V. K. N. Lau, "Sparse hybrid precoding for power minimization with an adaptive antenna structure in massive MIMO systems," *IEEE Trans. Wireless Commun.*, vol. 21, no. 7, pp. 5279-5292, Jul. 2022.
- [28] "Universal Mobile Telecommunications System (UMTS); Spatial channel model for Multiple Input Multiple Output (MIMO) simulations", 3GPP, Sophia Antipolis, France, Rep. TR 25.996, V11.0.0, Sep. 2012.
- [29] R. Cao, F. Gao, and X. Zhang, "A novel angular parameters estimator for incoherently distributed sources," in *Proc. Eur. Signal Process. Conf.*, Budapest, Hungary, Dec. 2016.
- [30] R. Liu, M. Li, Q. Liu, and A. Lee Swindlehurst, "DOA estimation-oriented joint array partitioning and beamforming designs for ISAC systems," *IEEE Trans. Wireless Commun.*, early access, Dec. 2024. doi: 10.1109/TWC.2024.3516037
- [31] Y. Sun, P. Babu, and D. P. Palomar, "Majorization-minimization algorithms in signal processing, communications, and machine learning," *IEEE Trans. Signal Process.*, vol. 65, no. 3, pp. 794-816, Feb. 2017.
- [32] A. Alkhateeb, O. E. Ayach, G. Leus, and R. W. Heath, "Channel estimation and hybrid precoding for millimeter wave cellular systems," *IEEE J. Sel. Topics Signal Process.*, vol. 8, no. 5, pp. 831-845, Oct. 2014.
- [33] J. Lee, G.-T. Gil, and Y. H. Lee, "Exploiting spatial sparsity for estimating channels of hybrid MIMO systems in millimeter wave communications," in *Proc. IEEE Global Commun. Conf. (GLOBECOM)*, Austin, TX, USA, Dec. 2014.
- [34] A. Ben-Tal and A. Nemirovski, *Lectures on Modern Convex Optimization: Analysis, Algorithms, and Engineering Applications* Philadelphia, PA, USA: Society for Industrial and Applied Mathematics, 2001.